LUND
UNIVERSITY

Master's Degree Project in

Department of Biology
Lund University

Functional connectivity analysis in the human brain using ultra-high field MRI

Theodor Rumetshofer

Master's degree project in Bioinformatics, 60 credits

Department of Biology, Lund University

2021

Supervisor: Peter Mannfolk and Olof Strandberg

Department of Clinical Science/Diagnostic Radiology, Lund University

Abstract

Introduction: Functional magnetic resonance imaging (MRI) is a non-invasive method which uses a combination of a strong magnetic field and radio frequency pulses to image magnetic difference between oxygenated and deoxygenated blood in the human brain. This contrast differences can be used to identify areas in the brain when subjects performing an active task in the MRI scanner. It is also possible to measure spontaneous BOLD oscillation in absence of an external stimuli, a method called resting-state fMRI (rsfMRI). However, it is necessary to estimated and remove physiological noise, like head movements or heartbeat, as well as MRI scanner noise. Those estimated signals are called confounds. Therefore, an accurate preprocessing of the time signals is necessary. However, available preprocessing pipelines are not well established yet for rsfMRI data from ultra-high field MRI scanners. The goal of this study was to compare two slightly different rsfMRI preprocessing pipelines on the same dataset. Further, to investigate the influence of these differences on the robustness and functional connectivity of specific resting-state networks (RSN).

Methods: A rsfMRI dataset from ten healthy subjects was acquired on an ultra-high field seven Tesla MRI scanner and preprocessed with both pipelines, CPAC and fMRIprep. A group-wise independent component analysis (ICA) was performed to measure the functional and spatial connectivity between and within RSN. Additionally, we performed a detailed comparison of the confounds between the pipelines.

Results: We identified six different RSN. Subjects preprocessed with fMRIprep showed a strong temporal correlation within the visual, sensory motor as well as between the left and right memory function network. However, there were no significant spatial differences between the pipelines. Although head motion confounds were similar, confounds using brain masks to extract the signal differ.

Discussion: The stronger positive and negative correlation is in line with the literature although the study lack in statistical power. The major impact of the pipeline differences could be addressed to varying brain masks from the estimated confounds. This detailed comparison may help to further investigate the influence of different preprocessing steps to functional connectivity.

Introduction

Magnetic resonance imaging (MRI) is a non-invasive method of studying neuroanatomical changes in the human brain. The combination of a strong magnetic field and radio frequency pulses make it possible to emphasize different contrasts between various brain tissues or fluids. One example is the difference between oxygenated and deoxygenated blood, which have diamagnetic and paramagnetic character, respectively. The paramagnetic deoxygenated blood causes local magnetic field distortions, which leads to a signal drop resulting in MRI images. Oxygenated blood will reduce these field distortions, yielding slightly higher signal. The differing signal strength between these two conditions is called blood-oxygen-level-dependent (BOLD) contrast (1). Differences in the blood flow and blood volume are mostly related to higher energy consumption in neuronal active brain regions by the neurovascular coupling (2). Although neuronal activity occurs on the scale of milliseconds, the BOLD response is slower and spanning seconds. The detected signal caused by the local field distortions is a complex interaction of cerebral blood flow and volume and can be detected by the MRI scanner using functional magnetic resonance imaging (fMRI).

A traditional fMRI experiment compares the BOLD response from a specific task to a baseline. Areas in the brain which are active during the task can be detected via the difference between the BOLD signals from the task and the baseline. One special case of fMRI is resting-state fMRI (rsfMRI) which measures spontaneous BOLD oscillations in absence of an external stimulus (3,4). Subjects are lying in the MRI scanner at rest with closed eyes, whereby the term "rest" means that the subjects are awake, without performing any task or thinking on something specific.

During rsfMRI (and also fMRI experiments) the whole brain is scanned repeatedly within 1-3 seconds with a voxel resolution of 1-4 mm^3 over several minutes resulting in one image volume at the given time point. Repeated over time allows to extract a time-series from each voxel in the brain. Two voxels in the brain which have similar time-series, i.e. they are correlated, are presumed to be functionally connected, and likely to process similar information (5). Large groups of voxels which exhibit a high functional connectivity at rest can often be characterized as forming a resting-state network (RSN). Several RSNs have been identified by their distinct spatial distributions in the brain, and their functionality deduced by comparing with activation patterns in task-driven fMRI experiments (5). The most common network is the default mode network (DMN) which can be identified only at rest. If a subject performs a task, the activation pattern of the DMN decreases. The state-of-the art method to identify such RSNs is the independent component analysis (ICA). ICA is an unsupervised and exploratory method which can be used to decompose the time-series in rsfMRI to identify spatial independent components (5).

The BOLD contrast measured in rsfMRI time-series is very small and it is a mixture of both neuronal and non-neuronal origin (6). The neuronal part of the signal is related to the local field distortions caused by deoxygenated blood (1). Non-neuronal signals are physiological fluctuations like heartbeat, respiration or noise from the MRI scanner (6). The key in preprocessing of rsfMRI data it to extract and remove the non-neuronal signal from the time-series. Extracted signals which contains noise are called confounds or nuisance signals. To minimize the effect of those confounds, a general linear model (GLM) is used to regress out those fluctuations from the time-series of each voxel in the brain, so-called nuisance regression. A multitude of different methods exists to extract those confounds from the time-series. Apart from these confounds, it is also necessary to correct for field inhomogeneities in the images

mostly caused at the boundaries between tissues or close to the sinuses in the brain. With susceptibility distortion correction (SDC) it is possible to correct for these inhomogeneities by generating a fieldmap. The fieldmap describes the displacement of a voxel in a certain direction.

To investigate the functional connectivity of the human brain rsfMRI is a well-established method. With the advent of faster image acquisition techniques and MRIs with higher field strength, from high field with 3 Tesla (3T) to ultra-high field with 7T, it is possible to increase the temporal and spatial resolution of rsfMRI images. Publicly available pipelines which are developed for the preprocessing of rsfMRI, are not well established yet for data from ultra-high field MRI. A recent work showed that the choice of the pipelines strongly varies between different sites although the same input data was used (7,8). Even the operating system (OS) on which neuroimaging pipelines are compiled and executed can have an impact on the output. Such differences also occur between versions of the same OS (9).

To investigate the impact of the preprocessing on the functional connectivity of 7T rsfMRI we applied the same dataset in two different pipelines. The goal of this retrospective study was to evaluate the impact of differences between the preprocessing pipelines and further to assess robustness of RSN. An additional goal of this work was to provide a reproducible study, due to the fact that many neuroimaging studies are lacking sufficient methodological detail (10,11). Therefore, in the following paragraphs we will give a detailed description of the preprocessing steps, aiming to understand the components underpinning rsfMRI reproducibility. This includes also a research resource identifier (RRID) for each applied software tool.

Material and Methods

Participants

Ten healthy individuals, all women with a median age of 45 (range= 30-55), were included in this study. The data was acquired within the frame of a study in Systemic Lupus Erythematosus at Lund University between June 2017 and February 2018. Inclusion criteria were: female sex, age between 18 and 55 years, right handedness, absence of autoimmune disease or any previous neurological or neuropsychiatric disorders. This study was approved by the Regional Ethical Review Board in Lund Sweden (#2012/4, #2014/748) and written informed consent was obtained for all subjects prior to inclusion.

Data acquisition

All subjects underwent a whole-brain scan on an actively shielded 7T MRI scanner (Achieva, Philips, Best, The Netherlands) using a 32-channel receive head coil (Nova Medical). Dielectric pads were used to reduce field inhomogeneities (12). The following sequences were included in this study: anatomical 3D T1-weighted (T1w) turbo-field echo sequence with a repetition time (TR)= 5 ms, Echo Time (TE) = 2 ms, Flip Angle (FA)= 6°, voxel size= 0.98 x 0.98 x 1 mm, slice spacing= 0.5 mm, field of view (FOV)= 256 x 256 x 380 and a parallel acquisition factor of 2 using sensitivity encoding (SENSE); rsfMRI was acquired with a 2D gradient-echo echo-planar imaging (EPI) sequence with a TR= 2300 ms, TE= 25 ms, FA= 73°, planar resolution= 0.9 x 0.9 mm, slice thickness= 2 mm, slice spacing= 0.2 mm, SENSE factor= 3, FOV= 256 x 256 x 45 and each functional run contained 202 volumes which resulted in an overall acquisition time of 8 minutes; to correct for B0 field inhomogeneities (susceptibility distortions) for the rsfMRI sequence phase difference and corresponding magnitude images

were additionally acquired (echo time difference= 1 ms). During rsfMRI the subjects were instructed to rest with their eyes closed.

Confounds

The most established confounds are the six head-motion parameters representing translation and rotation of the head during the rsfMRI scan in all three directions (13,14). From those six head-motion parameters, a summary statistic called framewise displacement (FD) was calculated for each imaged brain volume and captures the BOLD signal displacement (15). High-motion volumes which were above a certain FD threshold indicating a high movement and were removed from further analysis. Even small movements can have a strong impact on the connectivity analysis (16). Additional confounds were also extracted by averaging the time-series from the cerebrospinal fluid (CSF) as well as from the white matter (WM) in the brain. The latter contains the axons of the neurons and therefore less BOLD activation. Recently established methods like a temporal component-based noise pattern recognition method (tCompCor) derives a noise signal from voxels with a high standard variation, which were extracted using Principial component analysis (PCA) (17).

For nuisance regression the following confounds were removed from the time-series: six motion parameters as well as the first derivates and quadratic terms; average signal of the WM and CSF; tCompCor components which explains 50% of the variance. Additionally, tCompCor required a pre-calculation of low-frequency signal drifts (cosine filters) a prior, to filter physiological and MRI scanner related noise sources. Therefore, these cosine filters were also added to the nuisance regression.

Pipelines

In our comparison, two fMRI preprocessing pipelines, fMRIprep 20.2.0 (RRID:SCR_016216) (18) and CPAC 1.6.2 (RRID:SCR:000862) (19), were included in this study. The pipelines were used and executed inside a docker container using Docker 20.10.1 (RRID:SCR_016445). Both are based on Nipype 1.5.1 (RRID:SCR_002502) (20), an open-source Python interface which facilitates interactions between well-established neuroimaging software tools. Therefore, the underlying software tools and parameters were quite similar in both pipelines, however some steps were different. First, in CPAC the BOLD reference image to examine the motion parameters as well as the FD was defined as the mean image of all volumes instead of the first volume in fMRIprep. Second, different software tools were used to estimate the fieldmaps. Third, nuisance regression and bandpass filtering was performed in functional space for CPAC, compared to the standard space in fMRIprep.

It is necessary to mention that fMRIprep, provides an automatically generated boilertext of the different preprocessing steps. Parts of the following detailed description were taken from this provided text. However, this procedure is in line with the committee on publication ethics (COPE)[1], because it can be a helpful tool to increase the reproducibility of neuroimaging studies.

Preprocessing

An overview of the preprocessing steps in CPAC and fMRIprep as well as for their anatomical and functional branches can be seen in Figure 1.

[1] https://publicationethics.org/files/Web_A29298_COPE_Text_Recycling

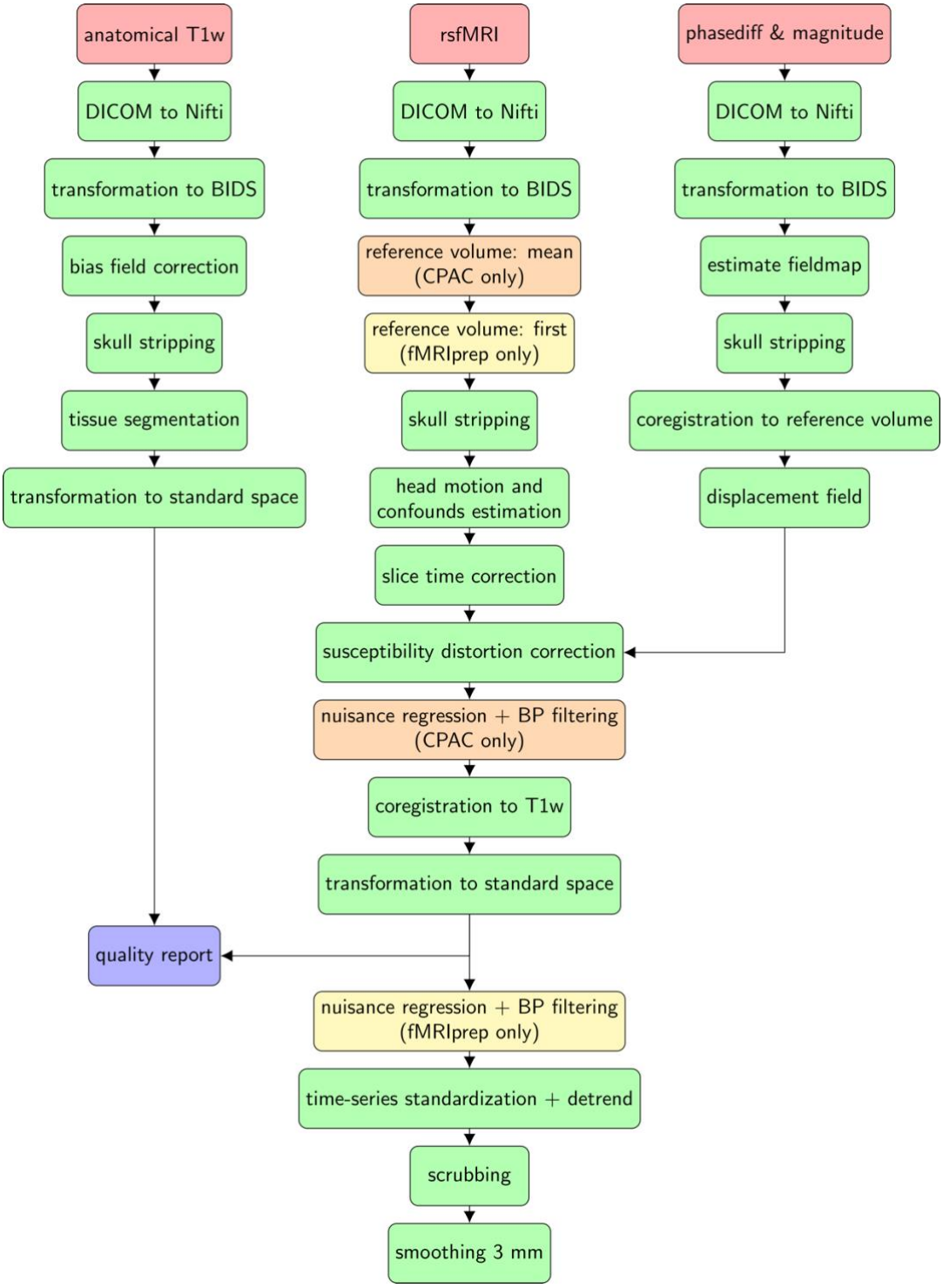

Figure 1. Workflow of the preprocessing steps. Steps which are equal in both pipelines are colored in green, for CPAC only in orange and for fMRIprep only in yellow. Both pipelines provide a quality report which is colored in blue. T1w= anatomical T1-weighted MRI sequence; DICOM= Digital Imaging and Communication in Medicine; Nifti= Neuroimaging Informatics Technology Initiative; BIDS= Brain Imaging Data Structure; BP= Bandpass; CPAC= Configurable Pipeline for the Analysis of Connectomes; fMRIprep= functional magnetic resonance imaging data preprocessing pipeline

The DICOM images were transferred to NIFTI-format using dcm2niix (21) and then transformed to Brain Imaging Data Structure (BIDS) (22) using an in-house developed Python script. All subjects were pre-processed with both pipelines.

For the anatomical preprocessing the T1w image was corrected for magnetic field inhomogeneities with N4BiasFieldCorrection (23), distributed with ANTS 2.3.3 (24) (RRID:SCR_004757) and used as T1w-references throughout the workflow. The T1w-references was then skull-stripped with Nipype implementation of the antsBrainExtraction.sh workflow (from ANTs), using OASIS30ANTs as target template. Brain tissue segmentation of CSF, WM and grey matter (GM) was performed on the brain-extracted T1w using fast (25) (FSL 5.0.9, RRID:SCR_002823). Volume-based spatial normalization to the ICBM 152 Nonlinear Asymmetrical template version 2009c (MNI152NLin2009cAsym) (26) (RRID:SCR_008796) was performed through nonlinear registration with antsRegistration (ANTs 2.3.3), using brain-extracted version of both T1w-reference and the T1w template.

For preprocessing the rsfMRI images, in fMRIprep the first volume was taken as a reference and its skull-stripped version was generated using a custom methodology of fMRIprep. The fieldmap was estimated based on the phase-difference map calculated with a dual-echo gradient-recall echo (GRE) sequences, processed with a custom workflow of SDCflows inspired by the epidewarp.fsl script and further improvements in Human Connectome Projects (HCP) pipelines (27). In CPAC the mean volume was used as a reference and 3dQWarp from AFNI 20160207 (RRID_SCR_005927) (28) was used to estimate the fieldmap. The fieldmap was then co-registered to the reference volume and converted to a displacement field map (amenable to registration tools such as ANTs) with FSL's fugue and other SDCflows tools.

Based on the estimated susceptibility distortion, a corrected EPI reference was calculated for a more accurate co-registration with the anatomical references. The BOLD reference was then co-registered to the T1w references using flirt (FSL 5.0.9) (29) with the boundary based registration (30) cost function. Co-registration was configured with nine degrees of freedom to account for distortions remaining in the BOLD reference.

Head-motion parameters with respect to the BOLD references (transformation matrices, and six corresponding rotation and translation parameters) are estimated before any spatiotemporal filtering using mcflirt (FSL 5.0.9) (31). Those six parameters were expanded with the inclusion of temporal derivatives and quadratic terms which resulted in 24 head motion parameters (14). BOLD runs were slice-time corrected using 3dTshift from AFNI. The BOLD time-series (including slice-timing correction when applied) were resampled onto their original, native space by applying a single, composite transform to correct for head-motion and susceptibility distortions. Several confounding time-series were calculated based on the BOLD: FD (31) and global signals extracted within the CSF and WM. Additionally, tCompCor (17) were estimated after low-frequency signal drifts from the top 2% variable voxels within the specific mask. Only tCompCor components which explains 50% of variance retained. All confounds calculated in those steps were placed within the corresponding confounds file.

In CPAC the BOLD time-series were bandpass filtered (0.01-0.1 Hz) and all above mentioned confounds were regressed out using a GLM. For both pipelines, the resulting filtered CPAC images as well as the unfiltered fMRIprep images, were resampled in MNI152NLin2009cAsym using the BOLD reference. Gridded (volumetric) resamplings were performed using antsApplyTransforms (ANTs), configured with Lanczos windowed sinc interpolation to minimize the smoothing effects of other kernels (32). For each pre-processed rsfMRI image a

whole-brain mask was also warped to the MNI152NLin2009cAsym space. In fMRIprep, the BOLD time-series in standard space were detrended, standardized, bandpass filtered (0.01-0.1 Hz) and all above mentioned confounds were regressed out in a nuisance regression using clean_image (NiLearn, RRID:SCR_001362) (33,34). However, the CPAC time-series were also detrended and standardized using clean_image from NiLearn in the standard space.

As a last step the BOLD time-series were smoothed using 3dmerge from AFNI with a 3 mm full width at half maximum (FWHM) blur kernel. The impact of the head motion was assessed for each subject using the FD.

Quality assessment

After the preprocessing a quality assessment was applied using an in-house developed Python script. To identify high motion subjects, one of the following exclusion criteria (35) needed to be fulfilled: i) mean FD > 0.25 mm, ii) maximum FD > 3 mm and iii) more than 25% of the functional volumes have FD > 0.4 mm. Subjects fulfilling one of these criteria needs to be completely excluded. This is also done in clinical studies otherwise they can have a strong impact on further analysis (35). For subjects which do not fulfil those exclusion criteria volumes which exceeded a FD value of 0.4 mm were removed from further analysis (scrubbing). This step is necessary to ensure that those high-motion subj do not influencing our ICA (35,36). Confounds used in the nuisance regression in both pipelines are per definition the same. However, differences can occur due to slightly different preprocessing steps. To investigate differences between those confounds, a Pearson correlation analysis was applied on the main confounds (6 motion parameters, tCompCor, CSF and WM mask) for each subject with an in-house developed Python script using statsmodel 0.10.1 (RRID:SCR_016074) (37).

Independent Component analysis

From all subjects, processed with CPAC and fMRIprep, the smoothed rsfMRI images were decomposed with a group-wise ICA into 20 statistically independent spatial components as implemented in the GIFT toolbox[2]. The data from different pipelines were set as different sessions for the analysis. Default parameters were applied in this analysis except for the brain mask which was generated by averaging the functional brain masks from all subjects using the generate mask utility in GIFT. To determine stability and reliability of the ICA algorithm, and therefore for the resulting components, ICA was performed 20 times using different initial values. The number of minimum and maximum cluster size was set to 16 and 20, respectively. This was done using ICASSO which is implemented in GIFT. The spatial patterns of the obtained independent components were visually inspected and associated to well-known resting state networks (38,39).

The functional or temporal connectivity was derived by a Pearson correlation analysis between each corresponding time-series from each component, derived over all subjects from a pipeline using the Python package statsmodel. All analyses used a z-score with a threshold of 1.96 as standard deviation, which correspond to a 95% confidence level. Furthermore, a voxel-wise paired t-test was applied to compare the spatial pattern of the RSN between CPAC and fMRIprep which is implemented in the GIFT utility SPM Stats. To correct for multiple comparison a Familywise Error Rate (FWE) with 0.05 was applied on the resulted T-map using statistical parametric mapping (SPM12) software (40) (RRID:SCR_007037).

[2] https://trendscenter.org/software/gift/

Results

The same set of subjects were pre-processed with two different preprocessing pipelines and analyzed together in a group-wise ICA. An example of a visual report from preprocessing from fMRIprep can be found in the GitHub repository[3].

Comparison of confounds

One subject was defined as a high-motion subject in both pipelines (mean FD > 0.36 mm and more than 38 % of the volumes have a FD > 0.4 mm). The subject showed a high frequent head motion in the translation as well as rotation in all three directions and was excluded from further analysis. As further necessary censorship apart from the complete subject exclusion, motion affected volumes also needs to be removed for each subject with a FD > 0.4 mm. The number of volumes which were removed for each subject and for each preprocessing pipeline can be seen in Figure 2. Volumes were removed only in four subjects. For two subjects, more volumes were removed in fMRIprep compared to CPAC and in one subject vice versa. The number of volumes removed in subject 4 were equal in both pipelines.

[3] https://github.com/TheoRum/master_project_bioinf

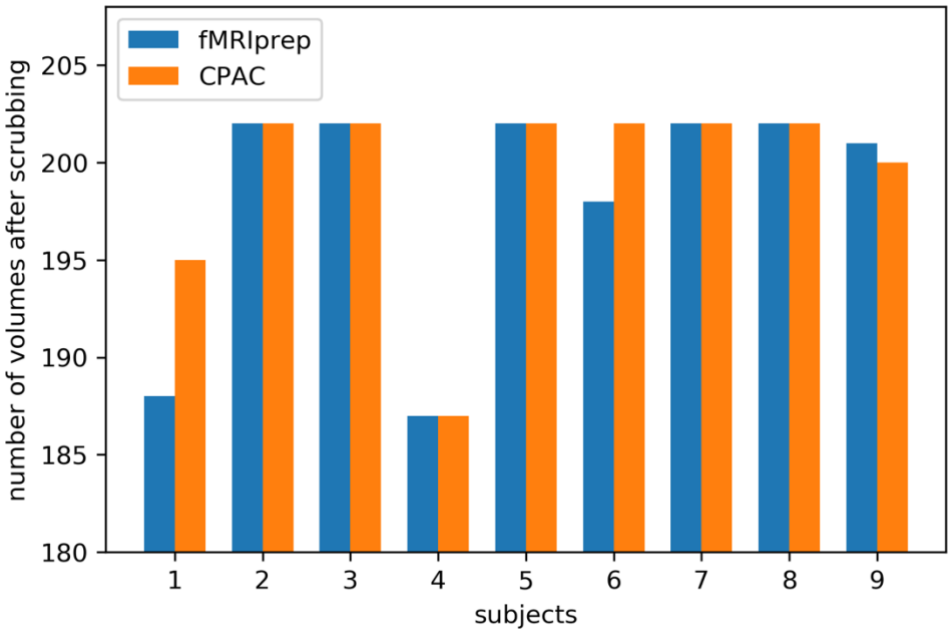

Figure 2. Number of volumes remained after scrubbing. In four of nine subjects, volumes were marked as outliers and removed from the time-series due to high FD values. FD= Framewise displacement; CPAC= Configurable Pipeline for the Analysis of Connectomes; fMRIprep= functional magnetic resonance imaging data preprocessing pipeline

Differences in the correlation coefficient of the confounds used in the nuisance regression between the different pipelines can be seen in Table 1. It is worth mention that the head-motion confounds from the translation and rotation in the y- and z-direction are interchanged in CPAC compared to fMRIprep. Additionally, the y-direction showed a negative correlation. However, all six head-motion parameters showed a very high correlation. In contrast, the averaged signal from the WM and CSF show a very low correlation value. This is the same for the tCompCor confounds, which are represented as one mean value over all components. CSF, WM and tCompCor using specific masks which can differ between the different pipelines. A comparison of the different masks used for those three confounds can be seen in Figure 3. Although all masks cover the same region of interest, i.e. WM, CSF and the voxels with the highest variability, the size and the areas differ between the pipelines.

SUBJECTS	01	02	03	04	05	06	07	08	09
Translation X	1.00	1.00	1.00	1.00	0.97	1.00	1.00	1.00	1.00
Translation Y	-1.00	-1.00	-1.00	-1.00	-1.00	-0.98	-1.00	-0.99	-0.95
Translation Z	1.00	1.00	1.00	1.00	1.00	0.99	0.99	0.99	1.00
Rotation X	0.99	0.99	1.00	0.98	1.00	0.99	1.00	0.99	0.99
Rotation Y	-0.98	-0.97	-1.00	-1.00	-1.00	-0.99	-0.99	-0.99	-1.00
Rotation Z	1.00	1.00	1.00	1.00	1.00	1.00	1.00	0.99	1.00
CSF	0.46	0.48	0.35	-0.27	0.58	0.28	0.18	0.36	0.78
WM	0.70	0.74	0.36	0.86	0.74	0.47	0.51	0.31	-0.12
tCompCor	-0.24	0.08	0.01	0.15	0.03	-0.04	-0.07	-0.01	-0.14

Table 1. Correlation of main confounds between the different pipeline for each subject. Head-motion for translation and rotation in y- and z-direction are interchanged in CPAC when compared to fMRIprep. The tCompCor components are averaged for each subject. CSF= Cerebrospinal fluid; WM= White matter; tCompCor= temporal PCA based noise reduction method; CPAC= Configurable Pipeline for the Analysis of Connectomes; fMRIprep= functional magnetic resonance imaging data preprocessing pipeline

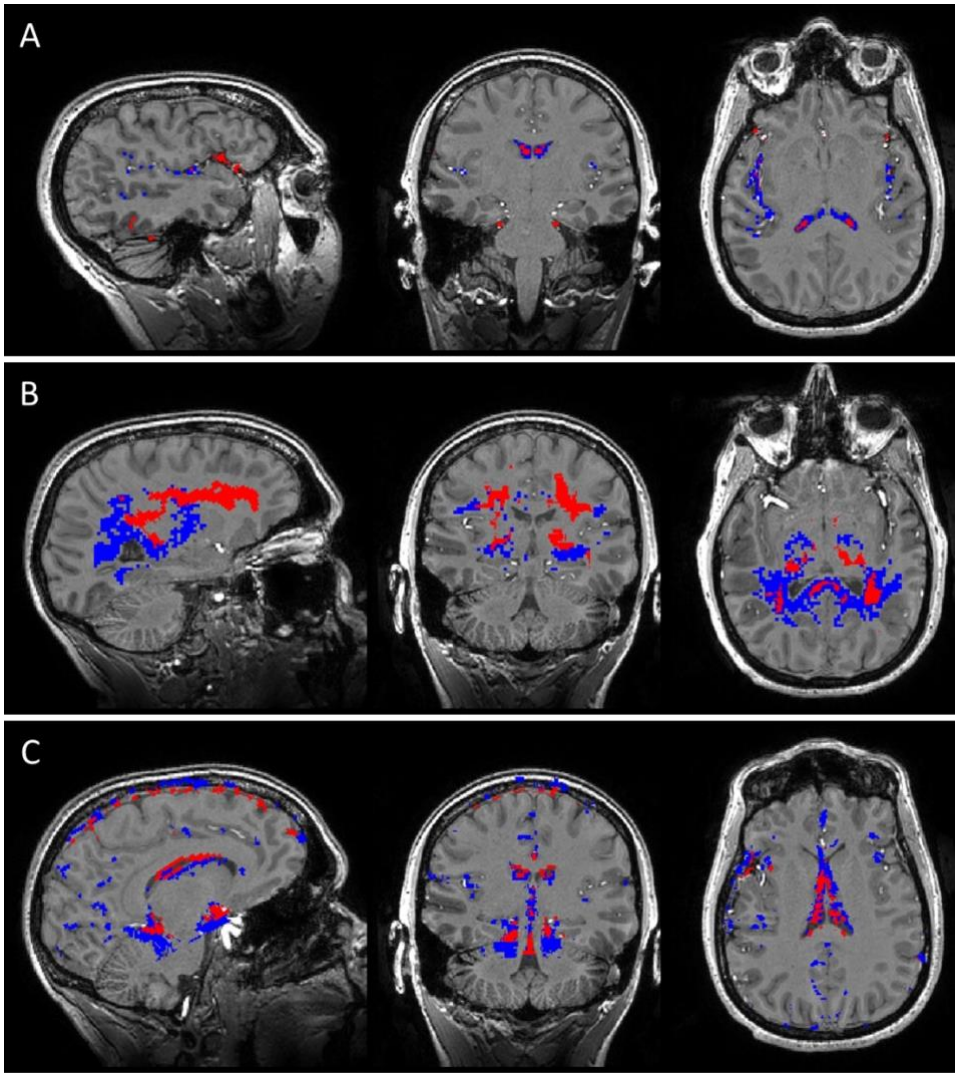

Figure 3. Comparison of confounds mask. Example of the masks used for the calculation of the confounds for CSF, WM and tCompCor from one subject**.** Masks used for CPAC are colored in blue whereas those from fMRIprep in red. A) Eroded CSF mask for CPAC covered beside the ventricles also areas between the temporal and frontal lobe of the brain. B) Eroded WM mask from CPAC covers the WM only in the posterior part of the brain, compared to fMRIprep which uses a mask over the whole WM in the brain. C) Voxel with the highest variability are chosen for the tCompCor mask which includes normally ventricles and areas close to large vessels. CPAC= Configurable Pipeline for the Analysis of Connectomes; fMRIprep= functional magnetic resonance imaging data preprocessing pipeline; CSF= Cerebrospinal fluid; WM= White matter; tCompCor= temporal PCA based noise reduction method

Susceptibility Distortion correction

Differences in the fieldmaps, which were generated by different tools within each pipeline could not be investigated. Due to internal processes the fieldmaps in CPAC were not saved in the output or working directory. Therefore, it was not possible to make a direct comparison between the two pipelines. However, an example of the fieldmap estimated with fMRIprep can be seen in Figure 4. Areas which are near to sinuses, in particular close to the nose and ears are merely displaced. The signal loss in these areas cannot be recovered, however some voxels can be returned to their original locations using those fieldmaps.

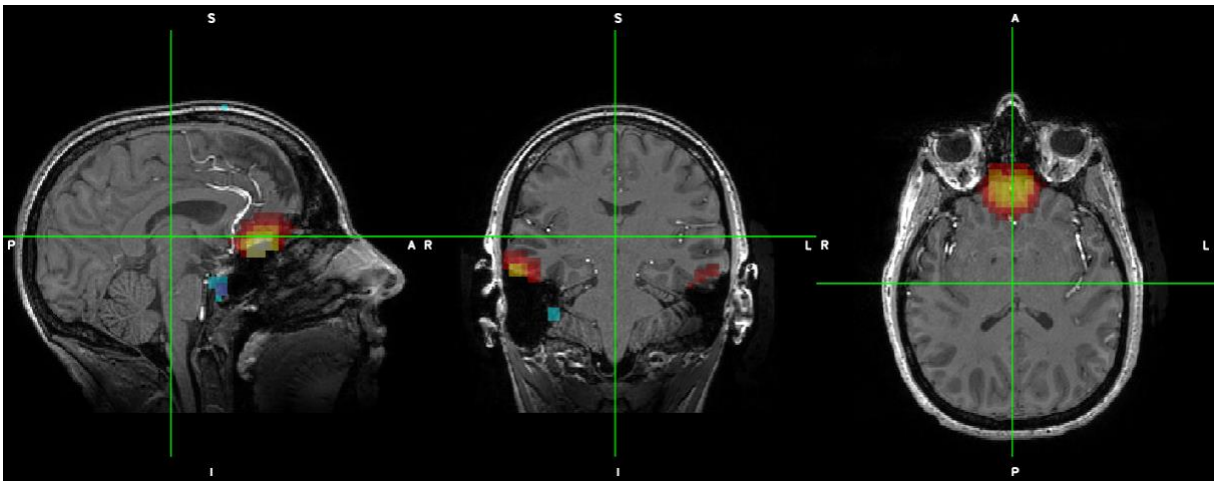

Figure 4. Fieldmap from one subject estimated with fMRIprep. Only voxels with an absolute displacement greater or equal than 1 mm are shown in color. Voxels which should be moved in the phase-encoding direction, i.e. to the frontal part of the brain, are shown in red-yellow whereas in the opposite direction are shown in blue. fMRIprep= functional magnetic resonance imaging data preprocessing pipeline

Group-wise ICA

The summary report from the group-wise ICA with 20 spatially independent components can be found in the GitHub repository[4]. After visual inspection 11 from 20 component calculated were associated to six well-known RSN (39,41): default mode network (DMN; component 13),

[4] https://github.com/TheoRum/master_project_bioinf

visual network (VIN; components 2,6 and 7), left memory function network (lMFN; 20), right memory function network (rMFN; component number 11), auditory network (AN; component 19) and a sensory motor network (SMN; components 3,4,5 and 12). An overview of those networks can be seen in Figure 5.

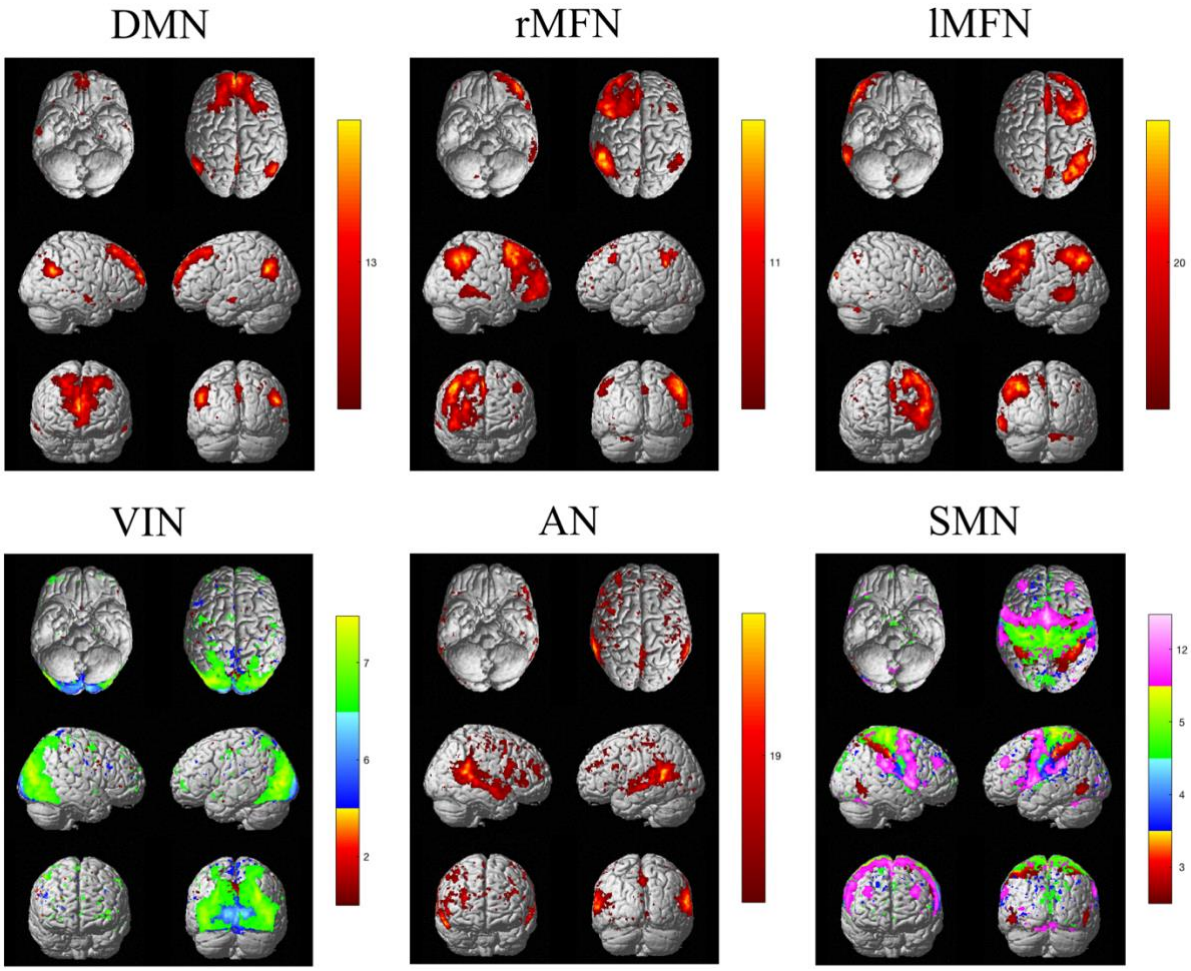

Figure 5. Overview of the selected RSN. Eleven ICA components were associated to six well-known RSN. The VIN and SMN consist of a combination of 3 and 4 independent components, respectively. All images are shown in standard-space. DMN= Default mode network; rMFN= right Memory function network; lMFN= left Memory function network; VIN= Visual network; AN= Auditory network; SMN= Sensory motor network; RSN= resting state networks; ICA= independent component analysis

The temporal connectivity of the selected components of the networks pre-processed with CPAC and fMRIprep is shown in Figure 6. The corresponding time-series from each component and subject were averaged and correlated. The components from subjects pre-processed with fMRIprep showed a higher correlation value within specific networks, e.g. VIN, SMN and between lMFN and rMFN, compared to CPAC. Furthermore, the DMN is stronger negatively correlated to SMN (12). However, there is also a stronger positive correlation from the AN to component 12 from the SMN. This can be also seen in the corresponding connectograms in Figure 7.

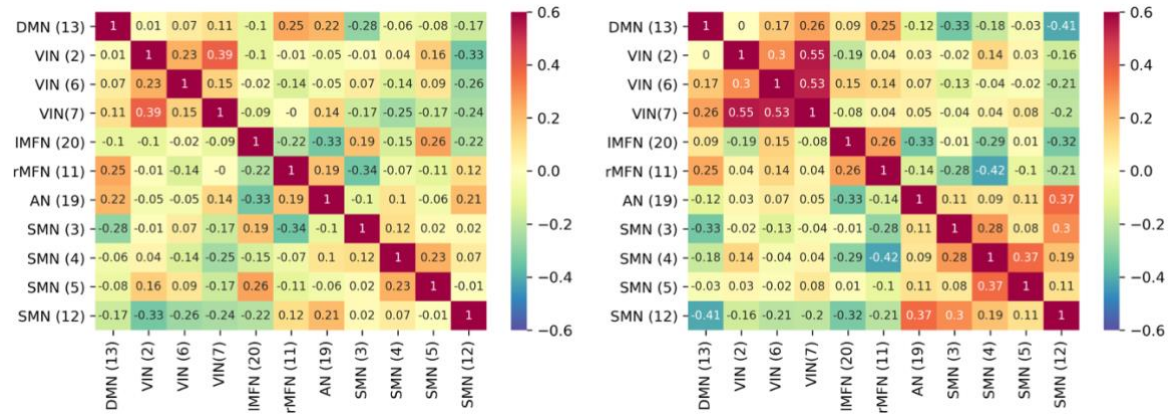

Figure 6. Correlation matrix of the ICA components. The matrix shows the chosen RSN with the corresponding component number. The components associated to the RSN are correlated for CPAC (left) and fMRIprep (right). The time-series are averaged over the subjects and correlated using Pearson correlation. DMN= Default mode network; rMFN= right Memory function network; lMFN= left Memory function network; VIN= Visual network; AN= Auditory network; SMN= Sensory motor network; RSN= resting state networks; CPAC= Configurable Pipeline for the Analysis of Connectomes; fMRIprep= functional magnetic resonance imaging data preprocessing pipeline

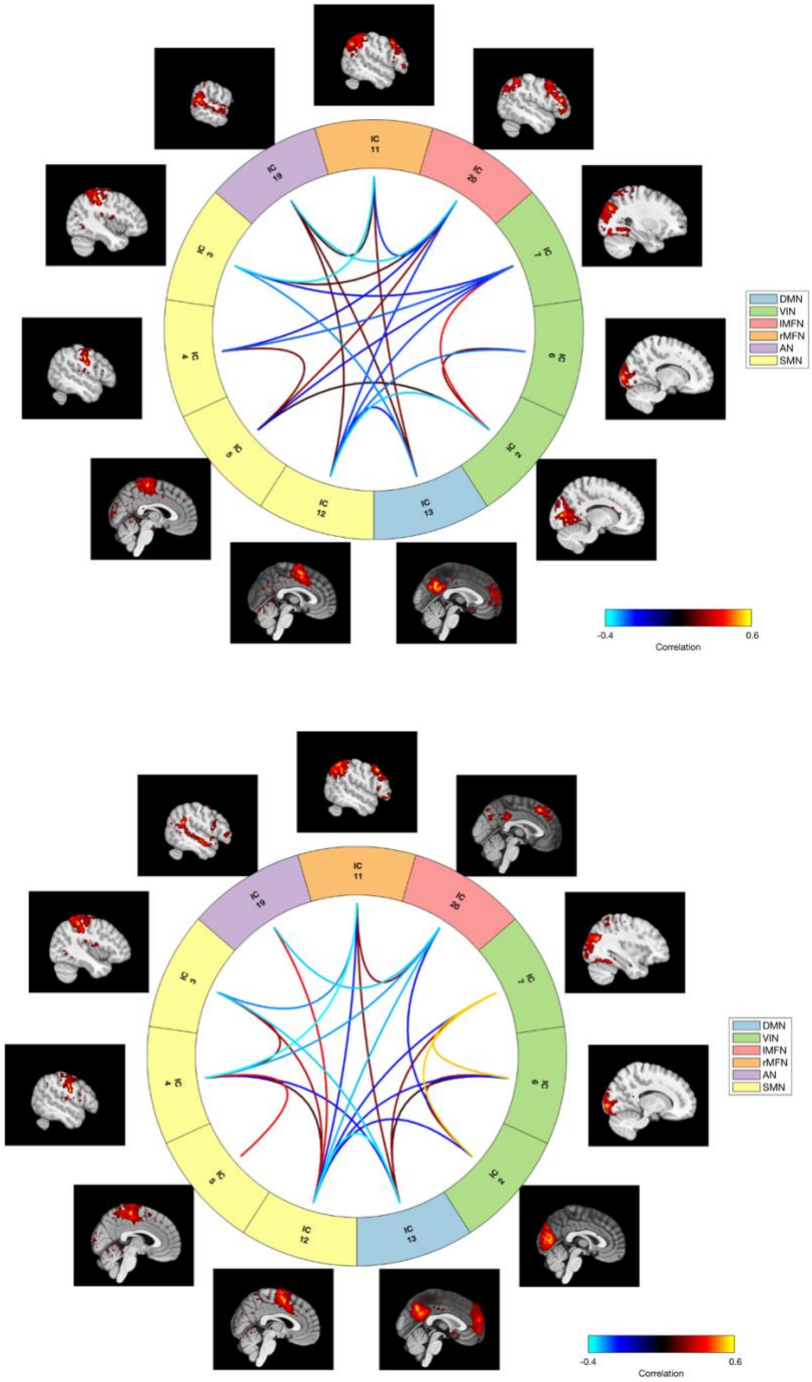

Figure 7. Connectograms of the different components. The ICA components are colored in the associated RSN the differences in the temporal connectivity between the components and RSN within the brain for CPAC (top) and fMRIprep (bottom) using Pearson correlation. Only correlation values with an absolute value > 0.15 are shown. DMN= Default mode network; rMFN= right Memory function network; lMFN= left Memory function network; VIN= Visual network; AN= Auditory network; SMN= Sensory motor network; RSN= resting state networks; CPAC= Configurable Pipeline for the Analysis of Connectomes; fMRIprep= functional magnetic resonance imaging data preprocessing pipeline

Differences in the spatial patterns of the eleven components between the pipeline were investigated using a paired t-test. Although contrasts of the ICA components in our RSN showed alterations, there was no significant differences between the two pipelines after multiple comparison. An example of the spatial activation pattern for the DMN for each pipeline as well as the contrast differences can be seen in Figure 8. A stronger activation contrast seems to occur in fMRIprep compared to CPAC, although those differences are not significant after FWR.

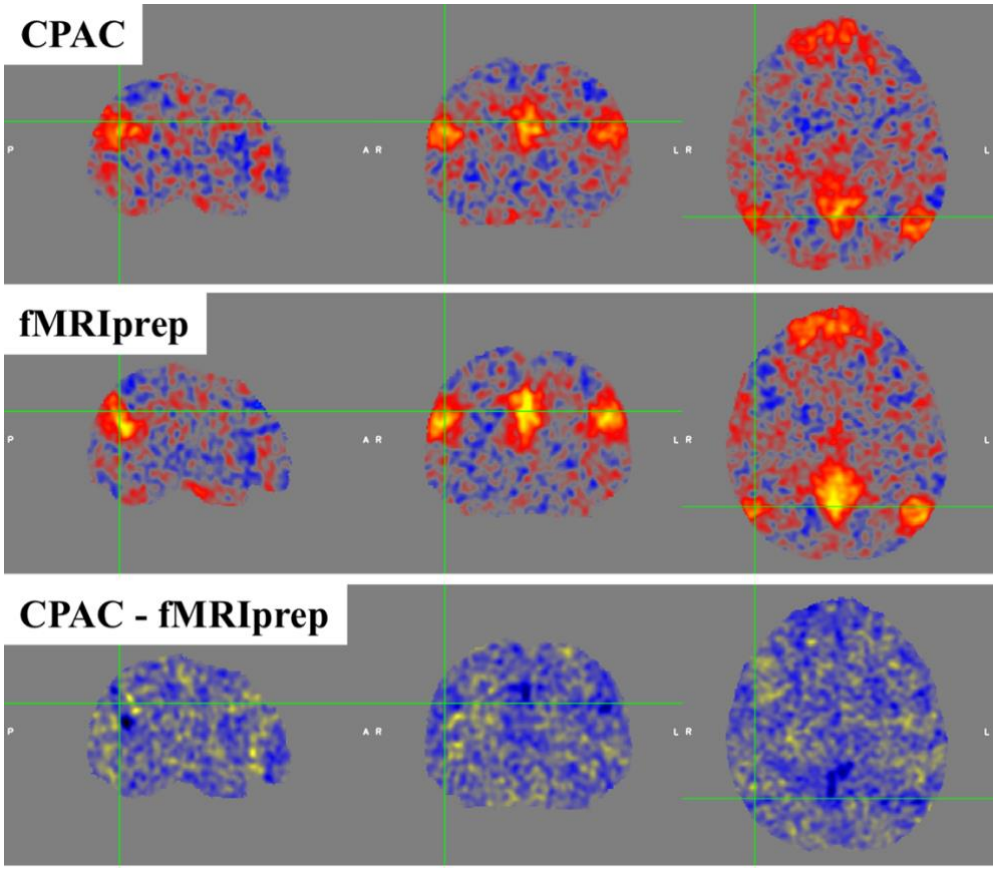

Figure 8. Activation map of the DMN. Activation map for the DMN for CPAC (top), fMRIprep (middle) and the subtraction (bottom), are shown. DMN= Default mode network; CPAC= Configurable Pipeline for the Analysis of Connectomes; fMRIprep= functional magnetic resonance imaging data preprocessing pipeline

Discussion

In this work, two rsfMRI preprocessing pipelines were evaluated on ten healthy subjects to identify differences in RSNs calculated with ICA. Six distinct RSN, which comprise eleven ICA components were extracted. Although there were no significant spatial differences in the components between the pipelines, the temporal connectivity between and within RSNs, were higher in subjects preprocessed with fMRIprep. Furthermore, we showed that less high-motion volumes were removed from subjects pre-processed in CPAC in two subjects. We also identified differences in the masks used to extract the confounds for CSF, WM and tCompCor.

Our main finding, an increase of temporal connectivity (Figure 6 and 7) needs to be set in context to the pipeline differences. First, the reference volume is a crucial part for calculating the six motion parameters and the FD (15). We found differences in the number of high-motion affected volumes between the pipelines using FD. Such volumes can have a strong impact on the statistical output of the analysis (15,42,43). In one third of our subjects, volumes needed to be removed and in two of the subjects more volumes were removed in fMRIprep and which would reduce the sensitivity to head motion (Figure 2). However, the number of volumes removed was small compared to the total number (max. 7%) although not all removed volumes were the same. Therefore, we suggest that the choice of the reference volume had only a minor effect on the higher temporal connectivity in the subjects pre-processed with fMRIprep. The change in volume-to-volume signal is calculated by the measure DVARS, which also is a well-established marker to detect high-motion volumes (15). The big advantage is that DVARS is calculated from volume to volume without including the six head motion parameters, which makes it independent from the choice of the references volume.

Second, the choice of the confounds for the nuisance regression model is an actively discussed issue in the literature and the relative merit of the choice varies a lot with the study design and the research question (35,36). Nevertheless, the confounds and also the preprocessing steps used in this study be considered by general consensus in the research field. The six head-motion parameters showed a clear correlation between the pipelines but differ in their orientation (Table 1). This permutation could not be fully tracked due to internal processes and co-registration from the reference volume. However, this permutation is consistent between the pipelines. One possible explanation could be the choice of the starting point from which the translation or rotation is calculation. It would make a difference in the starting point is the center of the reference volume or the edges. It is worth to mention that the FD value, which is calculated from the six head motion parameters, is highly correlated ($r > 0.91$) and significant ($p > 0.001$) with between the pipelines although the two parameters are interchanged.

Thirdly, the signal from the CSF, WM and large vessels in the brain were regressed out. Due to the fact that those areas do not contain any neuronal signal the extracted confounds used in the nuisance regression contains mostly physiological noise. The choice of the mask or ROI is a critical point (17). The more conservative a mask, the lower the probability to include neuronal signal which will be later removed from the time-series in the regression. Although both pipelines used eroded masks, the overlap seems to be small (Figure 3). As an example, the WM mask for fMRIprep is stretched over the whole WM in the brain whereas CPAC used mostly areas in the back. Further, from Figure 3 it stands out that the masks in CPAC have a lower resolution compared to fMRIprep, in particular 2 mm in all three directions compared to fMRIprep which uses masks in the original space of 0.9 x 0.9 x 2 mm. This increases the risk of a partial volume effect when a lower resolution is used. The choice of the ROI can have a strong impact on the extracted signals. These differences could have an impact on the lower

correlation between the confounds from the different pipelines and further on the functional connectivity.

Lastly, the impact of the estimated fieldmaps was not possible to compare. As mentioned above, the fieldmap from CPAC was not saved in the output or working directory. Nevertheless, a comparison of the fieldmaps from the subjects pre-processed with fMRIprep, showed a consistent pattern in terms of similar affected areas. The areas with the strongest correction by the SDC are mostly in the lower and frontal part of the brain (Figure 4). Therefore, if the influence of the different SDC methods will be applied, RSN which are close to those areas would be predominantly affected. However, the areas we identified with a higher temporal connectivity are mostly VIN, SMN, lMFN and rMFN and those are in the posterior and superior part of the brain. Additionally, both input for the tools estimating the fieldmaps (phase difference map and magnitude image) are the same for both pipelines. Nevertheless, it is worth to mention that the CPAC models does not give a full control of the data by not exporting the fieldmap. Due to the fact that, although the underlying software tools were different in the pipelines, both are based on the same input data and the impact on our results is expected to be small.

In general, the robustness of ICA on rsfMRI is a double-edged sword. It comes with a high level of robust RSN on a single-subject as well as on a group level. However, this robustness could be also a drawback, due to the fact that the influence of the pipeline differences does not have such a strong impact than we expected. Additionally, the lack of significant differences in the spatial pattern after multiple comparison is contrary to our increased temporal connectivity. However, voxels which show a higher contrast in the spatial maps might contribute higher to the time-course, although a significancy is not given after FWE correction.

One advantage of this study is that we used two pipelines which are based on Nipype. Also the underlying software packages and parameters were similar. This allowed a more controlled environment and reduces the impact of opaque internal processes in different packages. Further, both pipelines were executed on docker containers which reduces the influence specific libraries and increases the reproducibility of our results. It is worth to mention that although both packages are open-source software distributions it can be difficult to look deeper into internal processes due to the vast number of intermediate steps and calculations. As mentioned above, CPAC comes with a high degree of flexibility and it allows a variety of configurations by providing a pre- and postprocessing environment. This comes with some drawbacks, e.g. only confounds which are defined in the nuisance regression are exported. However, this inflexibility does not allow afterwards changes of confounds in the nuisance regression without starting the whole pipeline again. This can be a time issue if the working directories are not saved, which can be a problem due to the tremendous usage in hard drive space (around 80 GB per subject). fMRIprep, on the other hand, is less flexible and does only perform minimal preprocessing steps. However, it is using state-of-the-art software tools and exports all calculated confounds. This allows much more freedom in the composition of nuisance regression model and it gives more control of the following processing steps. As mentioned above, CPAC does not give this control due to the fact that the fieldmaps were not exported from the docker container.

A few limitations need to be addressed in this work. First, this analysis suffers in statistical power. Only ten subjects were included in this study and different types of analyses would be needed for a broader investigation of the influence of the pipeline differences. However, ICA was chosen due to the high reproducibility and robustness of the RSN (38,39). Second, only six

RSN which include eleven components were evaluate and a more selective numbers of components could unveil different RSN. Additionally, component 9 and 18, which were not included in our chosen RSN, could be assigned to the attention and executive control RSN (39,44). However, compared to the literature, their extracted contrasts do not cover all known parts of the brain. This example shows the dilemma of ICA which is that although it is an unsupervised method, it is necessary to define the number of components without knowing a ground truth. A too high number of components would split up RSN and a too low gives overlapping RSN. Additionally, at ultra-high field MRI there is a strong signal dropout due to field inhomogeneities in the lower and frontal parts of the brain. This loss of signal in our data limited our RSN to a certain extent. Third, this comparison was based on a specific choice of confounds which are regressed out from the time signal. A different nuisance regression with different confounds would be necessary to test the reproducibility of our results. However, this additional step would be beyond the scope of this work.

To conclude, we investigated the effect of specific preprocessing steps in two different rsfMRI pipelines using the same dataset. We showed that, although the pattern of the RSN derived by ICA were robust in both pipelines, the temporal connectivity differed. Overall, RSN from subjects pre-processed with fMRIprep showed a strong positive and negative correlation in general compared to CPAC. This detailed comparison may help to better understand the influence and interaction between different steps in the preprocessing of rsfMRI data at ultra-high field MRI.

Acknowledgements

The author thanks Peter Mannfolk and Olof Strandberg for the guidance through this project. Special thanks to Pia Maly Sundgren for this opportunity and her strong support.

References

1. Ogawa S, Lee TM, Kay AR, Tank DW. Brain magnetic resonance imaging with contrast dependent on blood oxygenation. Proc Natl Acad Sci. 1990 Dec 1;87(24):9868–72.
2. Logothetis NK, Auguth M, Oeltermann A, Pauls J, Trinath T. A neurophysiological investigation of the basis of the BOLD signal in fMRI. Nature. 2001;412(6843):150–7.
3. Biswal B, Zerrin Yetkin F, Haughton VM, Hyde JS. Functional connectivity in the motor cortex of resting human brain using echo-planar mri. Magn Reson Med. 1995 Oct;34(4):537–41.
4. Fox MD, Raichle ME. Spontaneous fluctuations in brain activity observed with functional magnetic resonance imaging. Nat Rev Neurosci. 2007 Sep;8(9):700–11.
5. Bijsterbosch J, Beckmann S, Smith C. Introduction to Resting State fMRI Functional Connectivity. Oxford Neuroimaging Prim. 2017;
6. Greve DN, Brown GG, Mueller BA, Glover G, Liu TT. A Survey of the Sources of Noise in fMRI. Psychometrika. 2013;78(3):396–416.
7. Botvinik-Nezer R, Holzmeister F, Camerer CF, Dreber A, Huber J, Johannesson M, et al. Variability in the analysis of a single neuroimaging dataset by many teams. Nature. 2020;582(7810):84–8.
8. Lindquist M. Neuroimaging results altered by varying analysis pipelines. Nature. 2020

Jun 20;582(7810):36–7.

9. Glatard T, Lewis LB, da Silva RF, Adalat R, Beck N, Lepage C, et al. Reproducibility of neuroimaging analyses across operating systems. Front Neuroinform. 2015;9(APR):1–14.

10. Carp J. The secret lives of experiments: Methods reporting in the fMRI literature. Neuroimage. 2012 Oct;63(1):289–300.

11. Poldrack RA, Fletcher PC, Henson RN, Worsley KJ, Brett M, Nichols TE. Guidelines for reporting an fMRI study. Neuroimage. 2008;40(2):409–14.

12. Teeuwisse WM, Brink WM, Webb AG. Quantitative assessment of the effects of high-permittivity pads in 7 Tesla MRI of the brain. Magn Reson Med. 2012 May;67(5):1285–93.

13. Friston KJ, Williams S, Howard R, Frackowiak RSJ, Turner R. Movement-Related effects in fMRI time-series. Magn Reson Med. 1996 Mar;35(3):346–55.

14. Satterthwaite TD, Elliott MA, Gerraty RT, Ruparel K, Loughead J, Calkins ME, et al. An improved framework for confound regression and filtering for control of motion artifact in the preprocessing of resting-state functional connectivity data. Neuroimage. 2013;64(1):240–56.

15. Power JD, Barnes KA, Snyder AZ, Schlaggar BL, Petersen SE. Spurious but systematic correlations in functional connectivity MRI networks arise from subject motion. Neuroimage. 2012;59(3):2142–54.

16. Power JD, Barnes KA, Snyder AZ, Schlaggar BL, Petersen SE. Steps toward optimizing motion artifact removal in functional connectivity MRI; a reply to Carp. Neuroimage. 2013 Aug;76:439–41.

17. Behzadi Y, Restom K, Liau J, Liu TT. A component based noise correction method (CompCor) for BOLD and perfusion based fMRI. Neuroimage. 2007;37(1):90–101.

18. Esteban O, Markiewicz CJ, Blair RW, Moodie CA, Isik AI, Erramuzpe A, et al. fMRIPrep: a robust preprocessing pipeline for functional MRI. Nat Methods. 2019;16(1):111–6.

19. Sharad S, Brian C, Ranjit K, Satra G, Chao-gan Y, Qingyang L, et al. Towards Automated Analysis of Connectomes: The Configurable Pipeline for the Analysis of Connectomes (C-PAC). Front Neuroinform. 2014;8.

20. Gorgolewski K, Burns CD, Madison C, Clark D, Halchenko YO, Waskom ML, et al. Nipype: A Flexible, Lightweight and Extensible Neuroimaging Data Processing Framework in Python. Front Neuroinform. 2011;5.

21. Li X, Morgan PS, Ashburner J, Smith J, Rorden C. The first step for neuroimaging data analysis: DICOM to NIfTI conversion. J Neurosci Methods. 2016 May;264:47–56.

22. Gorgolewski KJ, Auer T, Calhoun VD, Craddock RC, Das S, Duff EP, et al. The brain imaging data structure, a format for organizing and describing outputs of neuroimaging experiments. Sci Data. 2016 Dec 21;3(1):160044.

23. Tustison NJ, Avants BB, Cook PA, Zheng Y, Egan A, Yushkevich PA, et al. N4ITK: Improved N3 bias correction. IEEE Trans Med Imaging. 2010;29(6):1310–20.

24. Avants BB, Epstein CL, Grossman M, Gee JC. Symmetric diffeomorphic image registration with cross-correlation: Evaluating automated labeling of elderly and neurodegenerative brain. Med Image Anal. 2008;12(1):26–41.

25. Zhang Y, Brady M, Smith S. Segmentation of brain MR images through a hidden Markov random field model and the expectation-maximization algorithm. IEEE Trans Med Imaging. 2001;20(1):45–57.

26. Fonov VS, Evans AC, McKinstry RC, Almli CR, Collins DL. Unbiased nonlinear average age-appropriate brain templates from birth to adulthood. Neuroimage. 2009;47:S102.

27. Glasser MF, Sotiropoulos SN, Wilson JA, Coalson TS, Fischl B, Andersson JL, et al. The minimal preprocessing pipelines for the Human Connectome Project. Neuroimage. 2013;80:105–24.

28. Cox RW, Hyde JS. Software tools for analysis and visualization of fMRI data. NMR Biomed. 1997 Jun;10(4–5):171–8.

29. Jenkinson M, Smith S. A global optimisation method for robust affine registration of brain images. Med Image Anal. 2001 Jun;5(2):143–56.

30. Greve DN, Fischl B. Accurate and robust brain image alignment using boundary-based registration. Neuroimage. 2009 Oct;48(1):63–72.

31. Jenkinson M, Bannister P, Brady M, Smith S. Improved Optimization for the Robust and Accurate Linear Registration and Motion Correction of Brain Images. Neuroimage. 2002 Oct;17(2):825–41.

32. Lanczos C. Evaluation of Noisy Data. J Soc Ind Appl Math Ser B Numer Anal. 1964 Jan;1(1):76–85.

33. Abraham A, Pedregosa F, Eickenberg M, Gervais P, Muller A, Kossaifi J, et al. Machine Learning for Neuroimaging with Scikit-Learn. 2014;8(February):1–10.

34. Lindquist MA, Geuter S, Wager TD, Caffo BS. Modular preprocessing pipelines can reintroduce artifacts into fMRI data. Hum Brain Mapp. 2019;40(8):2358–76.

35. Parkes L, Fulcher B, Yücel M, Fornito A. An evaluation of the efficacy, reliability, and sensitivity of motion correction strategies for resting-state functional MRI. Neuroimage. 2018;171(December 2017):415–36.

36. Ciric R, Wolf DH, Power JD, Roalf DR, Baum GL, Ruparel K, et al. Benchmarking of participant-level confound regression strategies for the control of motion artifact in studies of functional connectivity. Neuroimage. 2017;154(March):174–87.

37. Seabold S, Perktold J. Statsmodels: Econometric and Statistical Modeling with Python.

In 2010. p. 92–6.

38. Beckmann CF, DeLuca M, Devlin JT, Smith SM. Investigations into resting-state connectivity using independent component analysis. Philos Trans R Soc B Biol Sci. 2005;360(1457):1001–13.

39. Damoiseaux JS, Rombouts SARB, Barkhof F, Scheltens P, Stam CJ, Smith SM, et al. Consistent resting-state networks. 2006;(2).

40. Nichols K. CHAPTER 20 - False Discovery Rate procedures. In: FRISTON K, ASHBURNER J, KIEBEL S, NICHOLS T, PENNY W, editors. Statistical Parametric Mapping. London: Academic Press; 2007. p. 246–52.

41. Smith SM, Fox PT, Miller KL, Glahn DC, Fox PM, Mackay CE, et al. Correspondence of the brain's functional architecture during activation and rest. Proc Natl Acad Sci U S A. 2009;106(31):13040–5.

42. Power JD, Mitra A, Laumann TO, Snyder AZ, Schlaggar BL, Petersen SE. Methods to detect, characterize, and remove motion artifact in resting state fMRI. Neuroimage. 2014;84:320–41.

43. Power JD, Schlaggar BL, Petersen SE. Recent progress and outstanding issues in motion correction in resting state fMRI. Neuroimage. 2015;105:536–51.

44. Beckmann C, Mackay C, Filippini N, Smith S. Group comparison of resting-state FMRI data using multi-subject ICA and dual regression. Neuroimage. 2009;47:S148.